

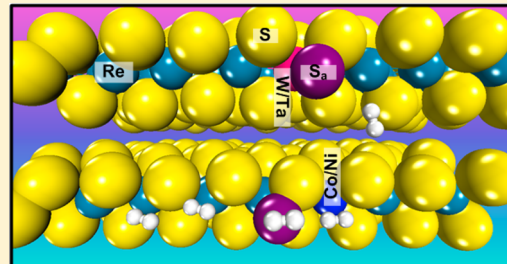
# Hydrogen Activation on the Promoted and Unpromoted $\text{ReS}_2$ (001) Surfaces under the Sulfidation Conditions: A First-Principles Study

Yucheng Huang,\* Hai Liu, Chongyi Ling, Xi Chen, Danmei Zhou, and Sufan Wang

Center for Nano Science and Technology, College of Chemistry and Material Science, The Key Laboratory of Functional Molecular Solids, Ministry of Education, Anhui Laboratory of Molecule-Based Materials, Anhui Normal University, Wuhu, 241000, Peoples' Republic of China

## S Supporting Information

**ABSTRACT:** Hydrogen activation on the promoted and promoter-free  $\text{ReS}_2$ (001) surfaces under the sulfidation conditions is studied by means of periodic density function theory (DFT) calculations within the generalized gradient approximation. First, surface-phase diagrams are investigated by plotting the surface free energy as a function of the chemical potential of S ( $\mu_S$ ) on the unpromoted and promoted  $\text{ReS}_2$  (001) surfaces with different loadings of nickel, cobalt, tungsten, and tantalum. The results show that on the unpromoted surface sulfur coverage of 25% and on the promoted surfaces sulfur coverage of 25% as well as 25% promoter modification are the most stable conditions, respectively, under hydrodesulfurization (HDS) reaction conditions. Second, hydrogen adsorption and dissociation are explored on these preferred surfaces. It is found that hydrogen adsorbs weakly on all the surfaces studied. The physical adsorption character makes its diffusion favorable, resulting in various adsorption sites and dissociation pathways, i.e., dissociation at surface Re or promote atom, at the interlayer, as well as at the adsorbed S atom. Calculated results show that hydrogen dissociation at the surface Re site is always kinetically favorable. All of the studied dopants can largely activate the adsorbed S but display distinct roles toward the activity of the nearest Re atom; i.e., Co/Ni dopant passivates the nearest surface Re while W/Ta activates it. The activity difference is found to be closely associated with the difference in the bond strength of metal–S and the resultant difference in the induced surface geometry. Moreover, promoter effect is localized because it seems nominal when the reaction occurs at a Re atom with one dopant atom separation. The present results provide a rational understanding of the activity difference between the promoter-free and the promoted surfaces, which would be helpful to further understand the mechanism of HDS and to enhance the development of highly active and selective hydrotreating catalysts.



## 1. INTRODUCTION

Research and development of appropriate and effective hydrodesulfurization (HDS) and hydrodenitrogenation (HDN) catalysts have drawn much attention due to environmental issues. Today, industrial emission from oil and gas becomes a major source of pollution due to existence of sulfur-/nitrogen-containing impurities. Since new environmental legislation requires the tolerance of sulfur content in oil products to be further reduced to less than 10 ppm, the production of clean fuels by the hydrotreatment process to remove sulfur/nitrogen from petroleum fractions has recently received increasing interest. Therefore, there is an emergent need for more efficient catalyzing processes and more active catalysts to meet the specifications. At present, the frequently used hydrotreatment catalysts in industrial plants are molybdenum- or tungsten-based sulfides with the promotion by nickel or cobalt,<sup>1–3</sup> which shows a high activity toward the removal of sulfur, nitrogen, and other impurities from oil fractions. The structures and properties of these catalysts have been extensively studied both theoretically and experimentally.<sup>4–8</sup>

In addition to Mo- and W-based catalysts, other sulfides can also be used on the petroleum refinement process. Chianelli et al.<sup>9</sup> found that the activity of metallic sulfides is different with the variation of transition metals, which displays “a volcano curve”. Among these, the activity order is believed to be as follows:  $\text{RuS}_2 > \text{Rh}_2\text{S}_3 > \text{PdS} > \text{MoS}_2 > \text{NbS}_2 > \text{ZrS}_2$ ;  $\text{OsS}_x > \text{IrS}_x > \text{ReS}_2 > \text{PtS} > \text{WS}_2 > \text{TaS}_2$ . In comparison to the traditionally used catalysts, precious metal sulfides show an obvious stronger activity. However, considering their cost and economics, these catalysts have little chance to be employed in the large industrial scale. In fact, other kinds of sulfides, i.e., rhenium sulfide, are often neglected. From the “volcano curve”, the activity of  $\text{ReS}_2$  is even higher than  $\text{MoS}_2$  and  $\text{WS}_2$ . It has been confirmed by Pakkanen et al.<sup>10</sup> that a 82.4% conversion of thiophene on  $\text{ReS}_2$  is observed, as compared to 69.0% on a commercial Co–Mo/ $\gamma$ - $\text{Al}_2\text{O}_3$  sample, indicative of a better catalytic property. To the best of our knowledge, the studies focusing on  $\text{ReS}_2$  catalyst are limited in the literature, especially

**Received:** March 20, 2015

**Revised:** June 27, 2015

**Published:** July 6, 2015

those on the promoter effects by theoretical means. Furthermore, their findings are quite different from each other.<sup>11–13</sup> For examples, Stern<sup>11</sup> reported that in the HDN process of indole and  $\alpha$ -ethylaniline Co addition decreases the activity of Re/ $\gamma$ -Al<sub>2</sub>O<sub>3</sub> catalyst but has a synergistic effect in the HDN of 2,3-dihydroindole. Rodin et al.<sup>12</sup> concluded that the Ni–Re pair supported over SiO<sub>2</sub> has an antagonism effect in thiophene HDS at atmospheric pressure. Escalona et al.<sup>13</sup> reported that unsupported Co–Re and Ni–Re mixed-sulfide catalysts prepared by the comaceration method exhibited a notable synergy effect in the HDS and HDN processes of gas oil.

Because of the lack of attention received and the considerable activity as well as a layered structure similarity to MoS<sub>2</sub> and WS<sub>2</sub>, ReS<sub>2</sub> catalysts have gained our great interest. Herein, by means of first-principles calculations, we disclosed a full account of investigation toward hydrogen activation on the Co-/Ni-/W-/Ta-promoted and unpromoted surfaces under the sulfidation conditions. Using a surface-phase diagram technique, we first obtained the structures and composition of the ReS<sub>2</sub> catalyst under the sulfidation conditions and then used hydrogen activation as a probe reaction to evaluate the promoter effect. We found that the 25% S adsorbed surface is not only stable from surface-phase diagram analysis but also robust in the sense that recovering the sulfided surface to a clean surface (without S adsorption) needs to surmount a substantial high energy barrier. Hydrogen can be easily activated at the Re site on all of the surfaces studied. The promoter effect, which can be rationalized by the bond strength of metal–S, is manifested on the nearest surface Re and the adsorbed S atom but does not embody on the farther atom.

## 2. COMPUTATIONAL METHODS AND THERMODYNAMIC MODEL

**2.1. Computational Methods.** All of the calculations were carried out by solving the Kohn–Sham equations with the Vienna ab Initio Simulation Program (VASP),<sup>14,15</sup> where electronic-ion interactions are described by the projector-augmented plane wave (PAW)<sup>16,17</sup> method. The generalized gradient approximation (GGA)<sup>18–20</sup> exchange-correlation functional of Perdew–Burke–Ernzerhof (PBE)<sup>18</sup> and a 400 eV energy cutoff for plane-wave basis set were used. The Brillouin zone sampling for gradient optimizations was carried out using a  $4 \times 2 \times 1$  grid, which is generated automatically using the Monkhorst–Pack<sup>21</sup> method.

We first optimized the ReS<sub>2</sub> crystal (triclinic, space group: P\bar{1}). The relaxed cell parameters show good agreement with the experimental values.<sup>22</sup> For the ReS<sub>2</sub> (001) surface, a large supercell ( $7.11 \times 12.85 \times 27.29 \text{ \AA}^3$ ) including one elementary ReS<sub>2</sub> unit in the  $x$  direction, two rows in the  $y$  direction, and three layers in the  $z$  direction was constructed (Figure 1). Note that, different from MoS<sub>2</sub>(100) surface where two inequivalent terminated orientations named Mo and S edges are presented, the atomic structures of the (10\bar{1}0) and (\bar{1}010) edges of the ReS<sub>2</sub>(001) surface are the same, exposing S atoms. During the structural optimization, the top layer was allowed to relax, while the bottom two layers were kept fixed at the bulk geometry.

Transition states were first located using the climbing nudge elastic band (CNEB)<sup>23,24</sup> method, and then were further optimized to the saddle point with the quasi-Newton algorithm. During the optimization of all the stationary points, the residual force acting on each atom was set to less than 0.03 eV/\text{\AA}. To characterize the transition states, frequency calculations were

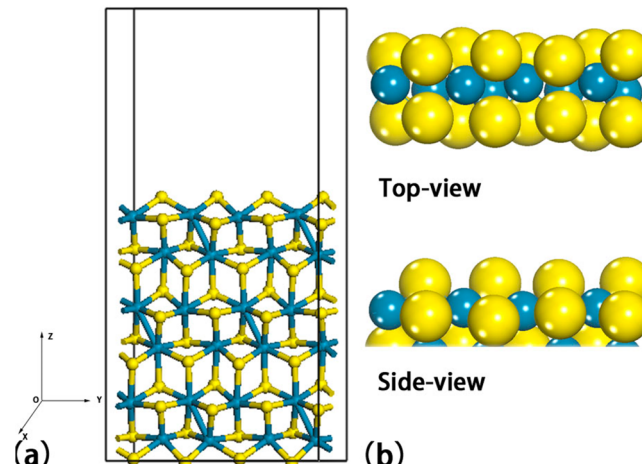


**Figure 1.** ReS<sub>2</sub> model representation consisting of six S–Re–S rows in the  $z$  direction and two units of supercells in the  $y$  direction (a). Top view and side view of the ReS<sub>2</sub>(001) surface (b). (Blue/yellow balls indicate rhenium/sulfur atoms.)

preformed. All of the TSs presented have only one imaginary frequency.

**2.2. Thermodynamic Model.** In previous studies, a general thermodynamic methodology has been employed<sup>25,26</sup> where a surface is in contact with a hydrogen sulfide atmosphere described by a hydrogen sulfide pressure  $p$  and temperature  $T$ . In this model, the H<sub>2</sub>S atmosphere can act as a reservoir, which is able to provide or reduce the number of hydrogen sulfide. We introduce the Gibbs free energy  $G$  ( $T, p, N_{\text{Re}}, N_S$ ) to describe the system as an appropriate thermodynamic potential. It is defined as

$$\gamma = \frac{1}{2A} [G_{\text{surface}}(\text{ReS}_2 + N_S \text{S}) - N_{\text{Re}}\mu_{\text{Re}} - N_S\mu_S] \quad (1)$$

Here,  $G_{\text{surface}}$  ( $\text{ReS}_2 + N_S \text{S}$ ) is the Gibbs free energy of ReS<sub>2</sub> and the adsorbed S (denoted as S<sub>a</sub> hereafter) in a unit cell.  $N_S$  and  $N_{\text{Re}}$  refer to the number of the atoms in the unit cell, and  $\mu_{\text{Re}}$  and  $\mu_H$  are the chemical potential of the Re and H, respectively.  $A$  is the area of the surface.

If the surface is large enough to act as a thermodynamic reservoir, the chemical potential is no longer independent.<sup>27</sup> Hence, the ReS<sub>2</sub> (001) surface will be in the thermodynamic equilibrium with bulk ReS<sub>2</sub>, that is

$$g_{\text{ReS}_2} = 4\mu_{\text{Re}} + 8\mu_S \quad (2)$$

where the lower case “ $g$ ” is used to represent the Gibbs free energy of the smallest structural unit of an infinite ReS<sub>2</sub> sheet. Inserting eq 2 into eq 1 leads to

$$\begin{aligned} \gamma = & \frac{1}{2A} \left[ G_{\text{surface}}(\text{ReS}_2 + N_S \text{S}) - \frac{N_{\text{Re}}}{4} g_{\text{ReS}_2} \right. \\ & \left. + (2N_{\text{Re}} - N_S)\mu_S \right] \end{aligned} \quad (3)$$

It is reasonable to assume  $g_{\text{solid}} \approx E_{\text{solid}}$  in which the contribution of vibration to the Helmholtz free energy is ignored. Then, the surface free energy becomes

$$\gamma = \frac{1}{2A} \left[ E_{\text{surface}}(\text{ReS}_2 + N_{\text{S}}\text{S}) - \frac{N_{\text{Re}}}{4} E_{\text{ReS}_2} + (2N_{\text{Re}} - N_{\text{S}})\mu_{\text{S}} \right] \quad (4)$$

Now, the surface free energy only depends on the sulfur chemical potential.

It should be noted that, under the sulfidation conditions, the value of  $\mu_{\text{S}}$  could be varied with bounds. If the sulfur chemical potential becomes too large, it will prefer to form bulk sulfur. Therefore, the upper bound can be written as

$$\mu_{\text{S}} \leq \mu_{\text{S}(\text{bulk})} \approx E_{\text{S}(\text{bulk})} \quad (5)$$

On the other hand, the free energy of the formation of  $\text{ReS}_2$  can be described as

$$\Delta G_f^{\text{ReS}_2} = g_{\text{bulk}}^{\text{ReS}_2} - 4\mu_{\text{Re}(\text{bulk})} - 8\mu_{\text{S}(\text{bulk})} \quad (6)$$

Combining this expression with eq 2 yields

$$\mu_{\text{S}} - \mu_{\text{S}(\text{bulk})} = \frac{\Delta G_f^{\text{ReS}_2}}{8} - \frac{1}{2}[\mu_{\text{Re}} - \mu_{\text{Re}(\text{bulk})}] \quad (7)$$

With the purpose for  $\text{ReS}_2$  to be stable against the formation of Re, here  $\mu_{\text{Re}} - \mu_{\text{Re}(\text{bulk})} \leq 0$  is also required to be tenable. Thus, the lower bound can be deduced from eq 7

$$\mu_{\text{S}} - \mu_{\text{S}(\text{bulk})} \geq \frac{\Delta G_f^{\text{ReS}_2}}{8} \quad (8)$$

$\Delta G_f^{\text{ReS}_2}$  can be calculated from the eq 9:

$$\Delta G_f^{\text{ReS}_2} \approx \Delta E_f^{\text{ReS}_2} = E_{\text{bulk}}^{\text{ReS}_2} - 4E_{\text{Re}(\text{bulk})} - 8E_{\text{S}(\text{bulk})} \quad (9)$$

Using the  $\alpha$  phase of sulfur for the evaluation of  $E_{\text{S}(\text{bulk})}$ , we calculated  $\Delta E_f^{\text{ReS}_2} = -7.0$  eV. Thus, the bounds of  $\mu_{\text{S}}$  are estimated to be

$$-4.97 \leq \mu_{\text{S}} \leq -4.09 \text{ eV} \quad (10)$$

In the cases of Co-/Ni-/W-/Ta-promoted surfaces, the free surface energy can be expressed as

$$\gamma = \frac{1}{2A} [G_{\text{surface}}(\text{promo} - \text{ReS}_2 + N_{\text{S}}\text{S}) - N_{\text{promo}}\mu_{\text{promo}} - N_{\text{Re}}\mu_{\text{Re}} - N_{\text{S}}\mu_{\text{S}}] \quad (11)$$

Here, "promo" represents a Co, Ni, W, or Ta atom. In previous studies,<sup>28,29</sup> the stability intervals for the Co and Ni sulfides are defined to be used as reference phases. Here, the  $\text{Co}_9\text{S}_8/\text{CoS}_2$  (pyrite phase) and  $\text{Ni}_3\text{S}_2/\text{Ni}_3\text{S}_4$  phases are considered for the references for Co and Ni, respectively.

Similar to the calculation for pure  $\text{ReS}_2$  surface, the free energy of the formation of  $\text{M}_x\text{S}_y$  is deduced from

$$\Delta G_f^{\text{M}_x\text{S}_y} = g_{\text{bulk}}^{\text{M}_x\text{S}_y} - x\mu_{\text{M}(\text{bulk})} - y\mu_{\text{S}(\text{bulk})} \quad (12)$$

Therefore, the lower bound follows

$$\mu_{\text{S}} - \mu_{\text{S}(\text{bulk})} \geq \frac{\Delta G_f^{\text{M}_x\text{S}_y}}{ny} \quad (13)$$

Here,  $n$  signifies the number of the  $\text{M}_x\text{S}_y$  units in the cell. Through the calculation we know that for  $\text{Co}_9\text{S}_8$  the inequation of  $\mu_{\text{S}} \geq -5.08$  eV need to be satisfied and for  $\text{CoS}_2$ ,  $\mu_{\text{S}} \geq -4.64$  eV. Therefore,  $\mu_{\text{S}} = -4.64$  eV is the boundary for  $\text{Co}_9\text{S}_8$  and

$\text{CoS}_2$ . For  $\text{Ni}_3\text{S}_4$ , it is required  $\mu_{\text{S}} \geq -5.11$  eV, and for  $\text{Ni}_3\text{S}_2$ ,  $\mu_{\text{S}} \geq -4.59$  eV. Accordingly,  $\mu_{\text{S}} = -4.59$  eV was the boundary for  $\text{Ni}_3\text{S}_4$  and  $\text{Ni}_3\text{S}_2$ .

### 3. RESULTS AND DISCUSSION

**3.1. Surface-Phase Diagram.** To evaluate the stabilities of the unpromoted and promoted  $\text{ReS}_2(001)$  surfaces with different ratios of sulfur coverage, the surface energy  $\gamma$  as a function of the chemical potential of sulfur  $\mu_{\text{S}}$  or  $p_{\text{H}_2\text{S}}/p_{\text{H}_2}$  ratios at 650 and 298.15 K are plotted, as shown in Figures 2 and 3.

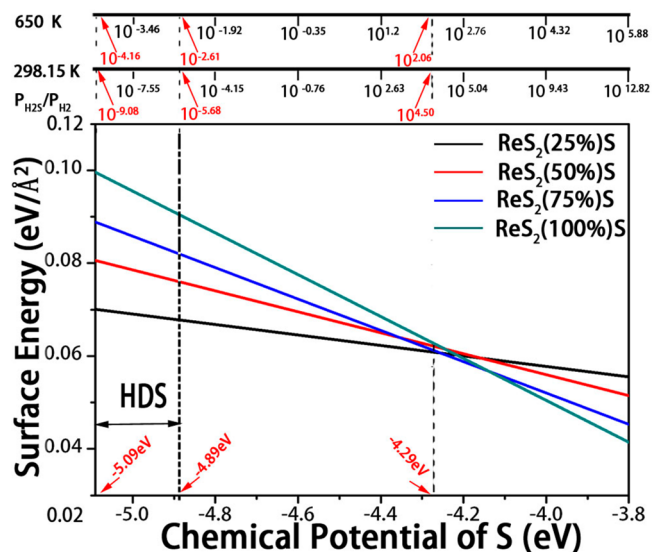


**Figure 2.** Surface energies of the unpromoted  $\text{ReS}_2(001)$  surface as a function of different sulfur coverage or  $p_{\text{H}_2\text{S}}/p_{\text{H}_2}$  ratios at 298.15 and 650 K. The experimental HDS condition is labeled with the vertical dotted line.

Here, the percentage of S is denoted as the ratio of  $S_a$  to the surface Re atoms. For example, 25% sulfur coverage refers to one sulfur atom adding to the surface (Figure S1, Supporting Information).

Specifically, Figure 2 illustrates the phase diagram of the promoter-free  $\text{ReS}_2(001)$  surface with different sulfur coverage. It can be seen that the structure with 25% sulfur coverage is the most stable when  $\mu_{\text{S}} < -4.29$  eV (corresponding to  $p_{\text{H}_2\text{S}}/p_{\text{H}_2} < 10^{2.06}$  and  $10^{4.5}$  at 650 and 298.15 K, respectively). With the increase of S chemical potential, the fully sulfided surface becomes favorable ( $p_{\text{H}_2\text{S}}/p_{\text{H}_2}$  ratio is larger than  $10^{2.76}$  at 650 K and  $10^{6.04}$  at 298.15 K, Figure 2). It is noteworthy that, at the experimental sulfidation conditions ( $\mu_{\text{S}} - \mu_{\text{S}(\text{bulk})}$ ) window is in the range from -1 to -0.8 eV<sup>30</sup>), 25% sulfur coverage is the most stable, in contrast to the  $\text{MoS}_2/\text{WS}_2$  system in which 50% S coverage (four adsorbed S atoms per surface) is proved to be optimal at the S-edge under similar conditions.<sup>8,30,31</sup>

Next, we turned our attention to the stable phase of the promoted surfaces. The formation energies, which are defined as  $E_f = E_{\text{promo}-\text{ReS}_2} + N_{\text{Re}}\mu_{\text{Re}} - E_{\text{ReS}_2} - N_{\text{promo}}\mu_{\text{promo}}$ , are calculated for the four modified surfaces, i.e., 25%, 50%, 75%, and 100% promoters' modifications. It was found that 25% Co-/Ni-/W-/Ta-substituted surface has the lowest formation energy. Thus, the 25% promoted surface is selected to further study the most stable phase with the variations of sulfur coverage. In comparison to the studies by Schweiger et al.,<sup>28</sup>

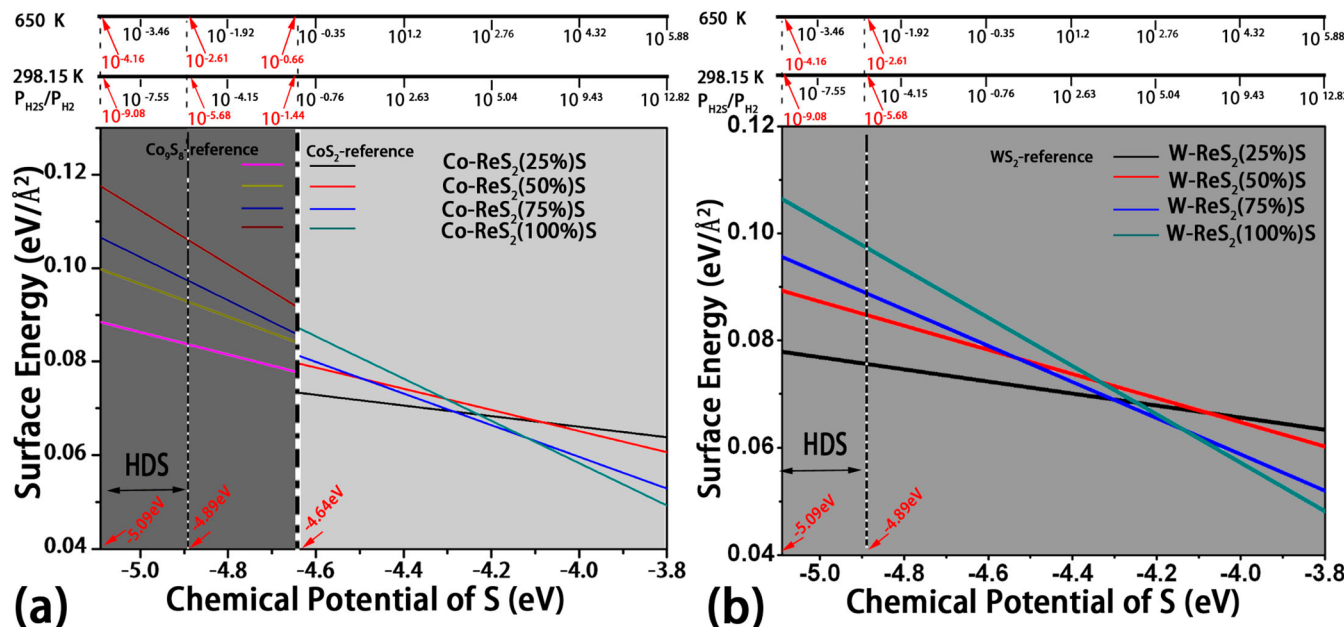


**Figure 3.** Surface energies of the Co-promoted  $\text{ReS}_2(001)$  surface as a function of different sulfur coverage or  $p_{\text{H}_2\text{S}}/p_{\text{H}_2}$  ratios at 298.15 and 650 K (a). The slope changes are due to different reference states for the Co sulfide phase (see text). (b) Surface phase of the W-promoted one. The experimental HDS condition is labeled with the vertical dotted line.

who used a full substitution of Mo atoms at the edge of  $\text{MoS}_2$  by the promoter atoms and by Krebs et al.,<sup>30</sup> and Girleanu et al.,<sup>31</sup> who extended to the cases where the promoted edge is substituted by several concentrations, only one promoter partial substitution was investigated in our study. The rationale is that the primary aim in this paper is to investigate the effect of promoter on  $\text{H}_2$  activation process rather than that of promoter concentration.

As shown in Figure 3a and Figure S2a (Supporting Information), the Co-/Ni-modified  $\text{ReS}_2$  surface phase diagram can be divided into two parts. The slope changes are due to different reference states for the Co/Ni sulfide phase. Because these two phase diagrams are similar, here we only describe the Co-modified one. When chemical potential  $-4.64 \leq \mu_S \leq -4.3$  eV, the 25% sulfidation is the most stable. When the chemical potential of sulfur is higher than  $-4.3$  eV, the most stable structure successively converts to 75% and 100% sulfidation (Figure 3a). On the other hand, as seen in the left panel of Figure 3a ( $\mu_S \leq -4.64$  eV), the surface energy always present a monotonous variation with the S coverage, that is, the less S coverage is, the more stable of the structure. In the case of W- and Ta-promoted surfaces, lack of different reference phases results in a linear character without break (Figure 3b and Figure 2Sb, Supporting Information). It is noted that the most stability is kept in 25% sulfidation in the chemical potential window of S under the traditional HDS reaction conditions, regardless of the dopants, which is the same to the promoter-free surface. On account of different structure, on the S-edge of  $\text{MoS}_2$  50% S coverage is reported to be most stable for 100% Co/Ni substitutions at the HDS conditions.<sup>30</sup>

**3.2. Hydrogen Adsorption and Dissociation.** On the basis of thermodynamic analysis, it was concluded that 25% S-covered  $\text{ReS}_2$  surface is the most stable under the HDS conditions. With modification by 25% Co, Ni, W, or Ta, 25% S adsorption also proved to be favorable. Further investigations toward hydrogen adsorption and dissociation on these surfaces

will address and disclose the promoter effect toward the catalyzing activity of  $\text{ReS}_2$ .

As expected, hydrogen bonds weakly to the surface as it is a saturated molecule. The calculated binding energies, which are defined as  $E_b = E_{\text{sub}} + E_{\text{H}_2} - E_{\text{sub/H}_2}$ , are all around 0 eV. Considering the dispersion contribution by using DFT-D2 method,<sup>32,33</sup> the magnitude of the  $E_b$  does not significantly improve. Thus, the high mobility enables hydrogen to occupy many potential sites for its dissociation. Here, three kinds of representative dissociation sites are selected, i.e., dissociation at surface Re or promote atom, at the interlayer and at the  $S_a$  atom. It is worth noting that on the pure  $\text{ReS}_2$  surface, four inequivalent Re atoms lead that four dissociation sites are available. In fact, one of the Re atoms is hidden behind the  $S_a$  atom, such that three surface Re atoms can be accommodated for hydrogen residence. Four promoted surfaces could fall into two classes: Because W and Ta justly locate behind the  $S_a$ , there are also three surface Re sites on the promoted surface. In contrast, on the Co- and Ni-promoted surfaces,  $S_a$  drifts to the Re atom, leaving the Co/Ni and two Re sites available (Figures 4–6). To be concise, thereafter we choose Co- and W-promoted surfaces to describe the hydrogen dissociation mechanism (Figures 5 and 6) and deposit the structures on Ni- and Ta-promoted surfaces in the Supporting Information (Figures S3 and S4).

**3.2.1. On the Promoter-Free Surface.** As seen in Figure 4, five initial states (IS) are selected: the first three ISs are hydrogen adsorption at the off-top Re site, i.e., on the right of  $S_a$  with the molecule plane paralleling to the Re–Re line (IS1), on the left of  $S_a$  with the angle of 52° (IS2), and next nearest to the  $S_a$  with the angle of 63° with respect to the Re–Re line (IS3), respectively. The fourth IS is hydrogen adsorption near the interlayer with the molecule plane vertical to the Re–Re line (IS4), and the last case is hydrogen adsorption at the top site of the  $S_a$  (IS5), where the plane of hydrogen is

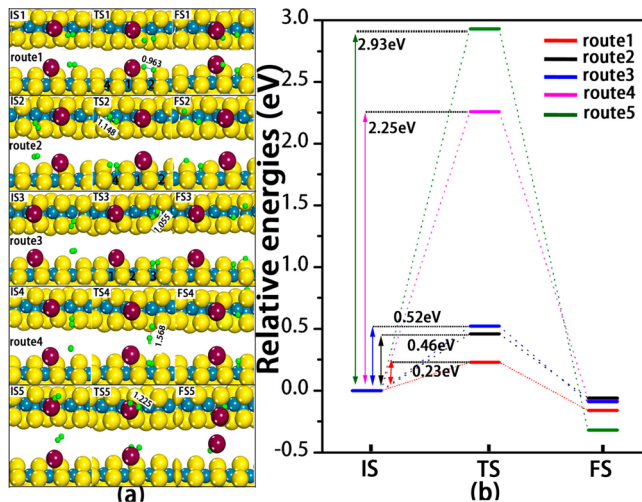


**Figure 4.** Structures of IS, TS, and FS for hydrogen dissociation on the promoter-free ReS<sub>2</sub>(001) surface (a). The labeled numbers are the H–H bond length (in Å). Potential energy surfaces of hydrogen dissociation (b). Blue, yellow, green, and purple balls represent Re, S, H, and the adsorbed sulfur atom, respectively.

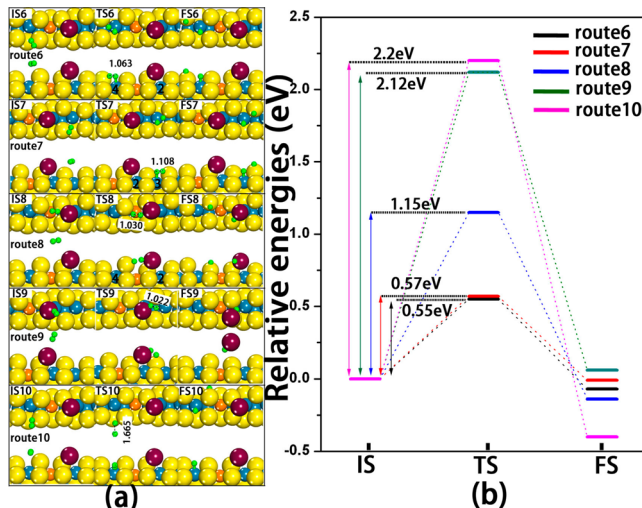


**Figure 5.** Structures of IS, TS, and FS for hydrogen dissociation on the Co-promoted ReS<sub>2</sub>(001) surface (a). The labeled numbers are the H–H bond length (in Å). Potential energy surfaces of hydrogen dissociation (b). Blue, yellow, green, purple, and orange balls represent Re, S, H, the adsorbed sulfur atom, and Co, respectively.

approximately vertical to the surface with the angle of  $\sim 67^\circ$  with respect to the surface normal.

Five possible adsorption systems correspond to five dissociation channels. As shown in Figure 4a, the H–H bond lengths gradually elongate and reach 0.963, 1.148, 1.055, 1.568, and 1.225 Å at the transition states (TS) along routes 1 to 5, respectively. Subsequently, for the first four pathways, one of the H atoms still leaves at atop site of the surface Re while another H atom migrates to the adsorbed/surface side S atom, leading to heterolytic dissociation with the formation of one Re–H group and one S–H group. By contrast, the fifth pathway of hydrogen dissociation occurs at the S<sub>a</sub>. With hydrogen molecule approaching to the surface and H–H bond length gradual stretching and being 1.225 Å, the TSS is formed. Then, H<sub>2</sub>S is generated in the gas phase, leaving a clean ReS<sub>2</sub> surface. Obviously, the kinetics of this pathway can be used as

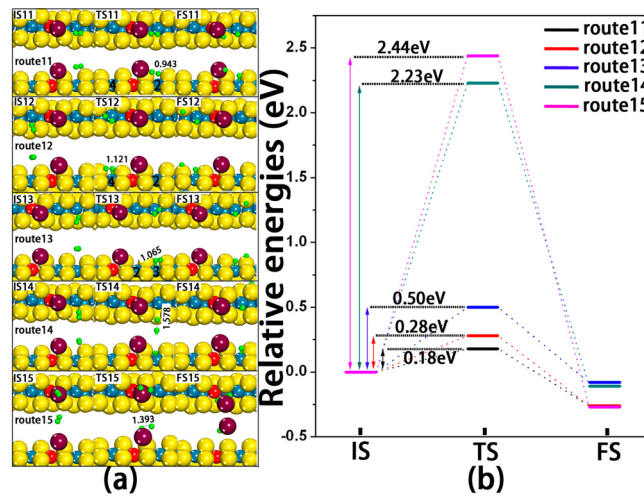


**Figure 6.** Structures of IS, TS, and FS for hydrogen dissociation on the W-promoted ReS<sub>2</sub>(001) surface (a). The labeled numbers are the H–H bond length (in Å). Potential energy surfaces of hydrogen dissociation (b). Blue, yellow, green, purple, and red balls represent Re, S, H, the adsorbed sulfur atom, and W, respectively.

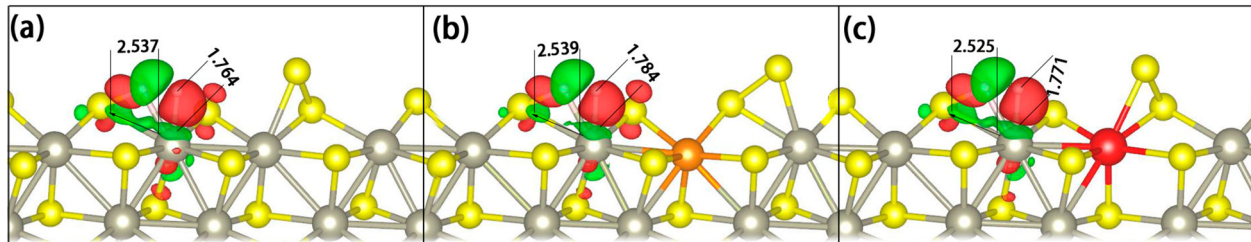
an indicator to evaluate the stability of the sulfided surface under the HDS conditions.

Figure 4b shows the reaction energy diagram for the hydrogen dissociation. It can be seen that all the studied channels are exothermic. The corresponding activation energies are calculated to be 0.23, 0.46, 0.52, 2.25, and 2.93 eV (Table 1). The reaction with the lowest energy

**Table 1. Geometrics ( $d_{\text{H}-\text{H}}$ , the H–H Distance in the TS), Energetic Information (Activation Energy  $E_a$ , Reaction Heat  $\Delta H$ ) for Hydrogen Dissociation on Promoted or Promoter-Free ReS<sub>2</sub>(001) Surfaces, and the p-Bond Centers of Selected S Atoms**

route	$E_a$ (eV)	$\Delta H$ (eV)	$d_{\text{H}-\text{H}}$ (Å)	p-bond center (eV)
1	0.23	-0.16	0.963	
2	0.46	-0.06	1.148	
3	0.52	-0.09	1.055	
4	2.25	-0.07	1.568	
5	2.93	-0.32	1.225	-2.37
6/6'	0.55/0.59	-0.07/-0.02	1.063/1.085	
7/7'	0.57/0.60	-0.02/0.00	1.064/1.083	
8/8'	1.15/1.08	-0.14/-0.16	1.030/0.999	
9/9'	2.12/2.16	0.06/0.09	1.022/1.143	-1.84/-1.89
10/10'	2.20/2.30	-0.40/-0.24	1.665/1.664	
11/11'	0.18/0.31	-0.26/-0.21	0.943/0.944	
12/12'	0.28/0.35	-0.26/-0.16	1.121/1.155	
13/13'	0.50/0.54	-0.08/-0.08	1.065/0.970	
14/14'	2.23/2.21	-0.27/-0.45	1.420/1.393	
15/15'	2.44/2.46	-0.11/-0.09	1.578/1.563	-1.88/-2.23

barrier is taken place at the surface Re site, where hydrogen is embraced by S<sub>a</sub>–Re<sub>1</sub>–Re<sub>2</sub> with an acute angle, demonstrating that hydrogen can be easily activated on the ReS<sub>2</sub>(001) surface (IS1 in Figure 4a). On the MoS<sub>2</sub> Mo-edge and S-edge with 50% S, hydrogen activation can also be readily achieved with barriers of 0.48 and 0.62 eV, respectively.<sup>34</sup> Comparing this pathway with route 2 (hydrogen locates inside an obtuse angle of S<sub>a</sub>–Re<sub>1</sub>–Re<sub>4</sub>), one can see that the structures of TS2 are not



**Figure 7.** Charge density difference of the TSs in the hydrogen dissociation process: (a) on  $\text{ReS}_2$  surface; (b) Co-modified and (c) W-modified  $\text{ReS}_2$  surfaces. The labeled number is the bond length (in Å). Green/red density regions represent charge accumulation/depletion. All of the isosurface values are set to be  $0.006 \text{ eV}/\text{\AA}^3$ .

effectively stabilized by the  $S_a$  but anchored by the side  $S$  (denoted as  $S_s$  hereafter), resulting in an increase in energy. The TS which is stabilized by the  $S_a$  adopts a nearly parallel configuration relative to the surface  $\text{Re}-\text{Re}$  line, while stabilization by the  $S_s$  takes a diagonal structure with respect to the two opposite side  $S$ . Due to geometry constraints and the more active nature of the  $S_a$ , one of the H in the TSs anchored by the  $S_a$  always possesses shorter H–H bond length and therefore has a lower dissociation barrier.

It is interesting that the barrier is rather sensitive to the location of the dissociated H in the TS. As far as hydrogen dissociation at the  $\text{Re}_3$  site is concerned, when the dissociated H locates on the  $S_s$  nearest to the  $S_a$  (not connected to  $S_a$ , lies between  $\text{Re}_2$  and  $\text{Re}_3$ , see Figure S5), the barrier increases to  $0.88 \text{ eV}$ , which is much higher than the present one ( $0.52$ ) along route 3. It is speculated that the next nearest  $S_s$  relative to the  $S_a$  has a more activity than the nearest  $S_s$ , which is a consequence of receiving less interaction from the  $S_a$ . This sensitivity makes us take especial cautions to the direction of the dissociated H for seeking other TS structures.

On the other hand, the substantial high-dissociation barriers at the interlayer and the  $S_a$  atom demonstrate that these two pathways are nearly prohibited. It should be noted that the larger barrier at the  $S_a$  indicates the adsorbed S is rather stable on the surface at the atmosphere of hydrogen (or high partial pressure of hydrogen) under the realistic HDS conditions.

**3.2.2. On the Co- and Ni-Promoted Surfaces.** On the Co-/Ni-promoted surface, the  $S_a$  atom does not exactly situate on the promoter but drifts to the nearest surface Re atom, indicating that Co-/Ni–S bonding is weaker than the  $\text{Re}-\text{S}$ .<sup>35,36</sup> Five stable adsorption configurations are located and five corresponding dissociation channels are explored accordingly (Figure 5 and Figure S3). Hydrogen dissociates at the surface Re nearest to the promoter Co/Ni ( $\text{Re}_4$ , route 6/6'), at the surface Re next nearest to the promoter Co/Ni ( $\text{Re}_3$ , route 7/7'), at the  $S_a$  (route 9/9'), as well as at the interlayer (route 10/10'), and hydrogen dissociation at the surface Co/Ni site is also identified (route 8/8', Figure 5 and Figure S3).

The spin-polarized calculations have to be taken into account as magnetic elements of Co/Ni involved in the system. Test calculations show that spin correction have essentially no effect on the barriers and reaction heats. Therefore, the reported values below are all the spin-uncorrected ones. The reaction at the Re site closest to the Co/Ni atom is initiated by the elongation of H–H bond length with a concomitant of molecule approaching to the surface (route 6/6' in Figure 5 and Figure S3). This reaction is slightly exothermic, and the calculated barrier is  $0.55/0.59 \text{ eV}$ . The configurations of this route can be deemed as the ones along the route 2, where the  $\text{Re}_1$  is substituted by the Co/Ni atom. Note that the

substitution results in  $S_a$  shifting from the first position of dopants to the second of Re atom. Numeric results show that the barrier is  $0.09/0.13 \text{ eV}$  larger than the one on the promoter-free surface, indicating the presence of Co/Ni passivates the nearest surface Re atom (Table 1). Intuitively, we seek the answer from the electronic property of Re. The calculated d-band centers, which are  $-1.58/-1.57$  and  $-1.69 \text{ eV}$  on the  $\text{Re}_4$  atom along route 6/6' and 2, respectively, seem incompatible with the variation of the activity. In fact, the stability of the TSs are not only determined by the surface Re but also are closely associated with the side  $S$ . As seen in Figures 7a and 6b, respectively, the charge density differences of TSs along routes 2 and 6 are plotted. It can be vividly seen that with Co modification the charge accumulation between H and Re, Re, and  $S_s$  decreases dramatically, accompanied by the increase of the bond length. Because of weaker bonding strength with the substrate, the TS along route 6 is less stable than the one along route 2. Thus, the barrier increase is a result of combined effect of Re and  $S_s$ . The passivation effect by Co/Ni modification was also reported by Travert et al.,<sup>37</sup> who calculated a barrier of  $0.79 \text{ eV}$  for Co-modified  $\text{MoS}_2$  Mo-edge (6a structure) versus a  $0.55 \text{ eV}$  for the promoter-free one (4b structure).

Route 7/7' describes hydrogen dissociation at the Re site, next nearest to the Co/Ni atom ( $\text{Re}_3$ , Figures 5a and S3a). It is expected that the dissociation would occur with the aid of the  $S_a$ ; therefore, the barrier should fluctuate around  $0.3 \text{ eV}$  (one along route 1). However, the energy barrier is calculated to be as high as  $0.57/0.60 \text{ eV}$  with near thermoneutrality (Figure 5b and Figure S3). In fact, it is unreasonable to compare with the route 1 in which the reaction site is formed by the acute angle of  $S_a-\text{Re}_1-\text{Re}_2$ , which is completely different from the case of this channel (the reaction site is constructed by the obtuse angle of  $S_a-\text{Re}_2-\text{Re}_3$ ). To reveal the effect of dopants, this pathway should be compared with route 3 in which  $\text{Re}_1$  atom is substituted by Co/Ni. Calculation results show that these two barriers are comparable (within  $0.08 \text{ eV}$ ); it is no surprise as the reaction site is a  $\text{Re}_2$  atom separation from the dopants.

Because Co/Ni is exposed on the surface, hydrogen dissociation at this site cannot be ignored. The structure of IS8/8' can be regarded as the IS1 in which the  $\text{Re}_1$  atom is replaced by the Co/Ni atom. The calculated energy barrier reaches  $1.15/1.08 \text{ eV}$  with slight exothermicity, largely higher than the one along route 1. Comparing the structures between TS8/8' and TS1, it is obvious that the barrier increment comes from the weaker interaction of Co-/Ni–H than  $\text{Re}-\text{H}$ , as the distances are measured to be  $2.59/2.67$  and  $1.85 \text{ \AA}$ , respectively. As a result, one of the dissociated H locates on  $S_s$  and the other migrates to  $S_a$  atom, respectively, at the FS8/8', leading to a hemolytic reaction on S–S pair. This kind of dissociation mode means that the reaction is independent of the dopants. In fact, a

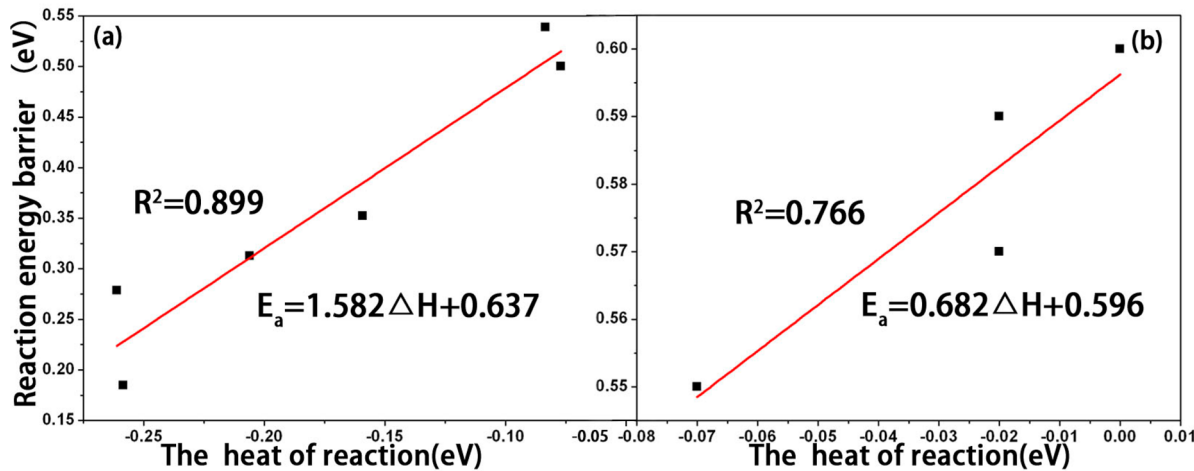


**Figure 8.** Relationship between energy barriers and reaction heats of hydrogen dissociation at the Re site: (a) on the W-/Ta-promoted surface, (b) on the Co-/Ni-promoted surface.

very low dissociation barrier for hydrogen was reported by previous theoretical studies on a pure Ni-/Co(111) surface.<sup>38,39</sup>

It is interesting that now the dissociation barrier at the  $S_a$  is no longer the highest one, but at the interlayer. Note that there is not much difference between the two magnitudes (barriers along routes 4 and 10/10') at the interlayer, indicative of a negligible effect of the Co/Ni in this case. This can be expected as the dissociated location is far away from the dopants. On the other hand, the barrier decreases to 2.12/2.16 eV at the  $S_a$ , which is 0.81/0.77 eV lower than the one on the promoter-free surface. Obviously, the sharp decrease is derived from the presence of dopants. Careful examination of partial density of states (PDOS) of the  $S_a$  shows that Co/Ni addition shifts the p orbital upward with respect to the Fermi level. This is consistent with the calculated p-band centers of S, which are -2.37 and -1.84/-1.90 eV on the promoter-free and Co-/Ni-promoted  $\text{ReS}_2$  surface, respectively. Here we can see that the further p-band center relative to the Fermi level, the higher the activation energy. This scenario agrees with the well-known thought of "d-band center model".<sup>40,41</sup> In fact, previous studies have been proved that the p-band center relative to the Fermi level can be used as a descriptor of catalytic activity in the design of new SOFC cathodes.<sup>42,43</sup>

**3.2.3. On the W- and Ta-Promoted Surfaces.** The bond strength of W-/Ta-S has been proven to be stronger than that of Re-S.<sup>35,36</sup> Thus, it is expected that the  $S_a$  is adsorbed at the dopants (W and Ta) rather than the Re atom on the  $\text{ReS}_2$  surface. However, energetics results show that it is somewhat slightly less stable than the one where the  $S_a$  settles on the nearest Re atom, viz., adopting that sort of Co/Ni model. The comparable total energy indicates these two models have an equal opportunity to occur. We are more interested in the expected model because the surface configuration is totally different from the Co/Ni-doped one. Obviously, investigation on this model can determine whether the exposure of dopants is beneficial to the activity or not. Because of their similar surface morphology, hydrogen dissociation on the W-/Ta-promoted surface follows the same pathways as on the promoter-free  $\text{ReS}_2$  surface.

As shown in Figure 6 and Figure S4, the reaction is nearly neutral along route 11', while it is exothermic along the remaining routes. The corresponding energy barriers are calculated to be 0.18/0.31, 0.28/0.35, 0.50/0.54, 2.23/2.21,

and 2.44/2.46 eV along the routes 11/11'-15/15', respectively (Table 1). Resembling to the routes 1–3, dissociation at the surface Re site (routes 11/11'-13/13', Figure 6a and Figure S4) needs the aid of either the  $S_a$  or the  $S_s$  atom. Still, the lowest barrier occurs at the Re site on the acute angle side of the  $S_a$  with a paralleling dissociation mode (route 11). The calculated barrier is 0.18/0.31 eV, comparable with the one along route 1 (0.23 eV,  $\pm 0.08$  eV deviation), demonstrating that (i) hydrogen is readily dissociated at Re site and (ii) the presence of W/Ta has nominal effect on the activity of the right Re. The latter is understandable because there is the  $S_a$  atom separation between dopants and  $\text{Re}_2$  (W-/Ta-Re<sub>2</sub> distances: 3.70 and 3.77 Å); therefore, the aided  $S_a$  determines the dissociation kinetics. Naturally, one can imagine that the effect of W/Ta may focus on the obtuse side of  $S_a$ . Indeed, the dissociation becomes kinetically and thermodynamically favorable. As illustrated in Figure 6b and Figure S4b, hydrogen dissociation has an energy barrier of 0.28/0.35 eV, which is 0.18/0.11 eV lower than the corresponding one on the promoter-free surface, indicating that the presence of W/Ta activates the nearest Re atom. The influence of the W/Ta turns weaker when the reaction occurs at the Re site next neighboring to the dopants (route 13/13'). The calculated barrier is 0.50/0.54 eV, which is comparable with the one (0.52 eV) on the promoter-free surface, as expected.

To understand the promoter effect of W/Ta, the charge density difference of TS along route 12 is drawn in Figure 7c. With a comparison to the one on the promoter-free surface, the charge accumulation between Re and  $S_s$  increases while it is nearly invariant between Re and H as indicated from the variation of bond length. The stronger bonding is beneficial for the stability of the H···H entity, resulting in more favorable dissociation.

Finally, similar to the pathways on the promoter-free and the Co-/Ni-promoted surfaces, hydrogen dissociation at the interlayer and the  $S_a$  site is also under consideration. Calculated results show that in order for the sulfided surface to recover to the clean surface a barrier of 2.44/2.46 eV must be conquered, which is much lower than the one on the promoter-free surface but higher than that of the Co/Ni-promoted surfaces. It is understandable as the p-band center is computed to be -1.88/-2.23 eV, so it also falls in between the values for the promoter-free and Co/Ni surface. In contrast, the interlayer

dissociation has nearly nothing to do with the presence of promoter. The calculated barrier is 2.23/2.21 eV, close to the ones on the other two surfaces.

In Figure 8 are plotted the correlations between energy barriers and reaction heats. Data collected from the first three pathways on the W-/Ta-promoted surface and the first two on the Co-/Ni-promoted are drawn in parts a and b, respectively, of Figure 8. It can be seen that the correlation coefficient square reaches 0.899 and 0.766, indicating that the reaction heat can be used as descriptors to measure the activity of the hydrogen dissociation, which is known as a “Brønsted–Evans–Polanyi (BEP) relationship”.<sup>44,45</sup>

The above hydrogen dissociations at various sites on the promoter-free and Co-, Ni-, W-, and Ta-promoted surfaces have been systematically investigated. We show that the presence of promoters has a notable effect on the  $S_a$  and the nearest Re atom, which is not separated by the  $S_a$  atom, but has a nominal effect on the next nearest Re and the farther atoms. When the reaction occurs at the nearest Re site with respect to the dopants, the dissociation of hydrogen on the Co-/Ni-modified  $\text{ReS}_2$  surface is hindered, while the W-/Ta-modified one reinforces the activity.

It is interesting that two kinds of different promoters display distinct roles toward activity. On the Co-/Ni-promoted surface, because the Re–S bond strength is larger than the Co–Ni–S, the  $S_a$  locates on the surface Re atom rather than Co/Ni site. This scenario is consistent with previous studies on Co-/Ni-promoted  $\text{MoS}_2$  surfaces.<sup>34,37</sup> As W-/Ta–S is stronger than the Re–S, the  $S_a$  is calculated to have an equal possibility to adsorb on either the dopants or the Re site. The different bond energy brings different surface morphology as well as a different promoter effect: on the Co-/Ni-modified surface, the promoter pushes the  $S_a$  to the nearest Re atom at that moment the promoter atom is exposed, and it deactivates the nearest Re atom but activates the  $S_a$ . On the studied W-/Ta-modified surface, however, the promoter is shielded by the  $S_a$ , and its effect on the  $S_a$  is decreased compared with the Co-/Ni-doped one, but the nearest Re atom is activated. Thus, it is safe to assume that the promoter effect toward activity is closely associated with the bond strength of M–S (M = Re/Co/Ni/W/Ta) and thus induced surface geometry difference. In Figure 9, we try to correlate M–S bond energy as a function of the energy barrier; it is surprising that not only the assumed regularity is held but also a considerable linear relationship is obtained. This result indicates that choosing a promoter with strong bond strength with S can activate a nearby Re atom on the parent catalyst. Moreover, one can artificially modulate the activity of hydrogen dissociation by alloying with different metals. This may be of important significance to the design and further optimization of more effective hydrotreatment catalysts.

It should be noted that the promoter effect reported here seems to be contradicted by the well-established existence of a volcano curve in that the highest HDS activity can be achieved with an optimized M–S bond strength.<sup>36</sup> Actually, when hydrogen dissociation is used as a probe reaction, the promoter effect revealed here may not be applied to the whole HDS/HDN process since hydrogen activation is not necessarily the rate-limiting step on transition-metal sulfides. However, understanding hydrogen dissociation behavior is a basis for the research of HDS and HDN catalysts. We believe the present work not only leads to a more rational understanding of the catalytic active transition metal sulfide phase but also gives

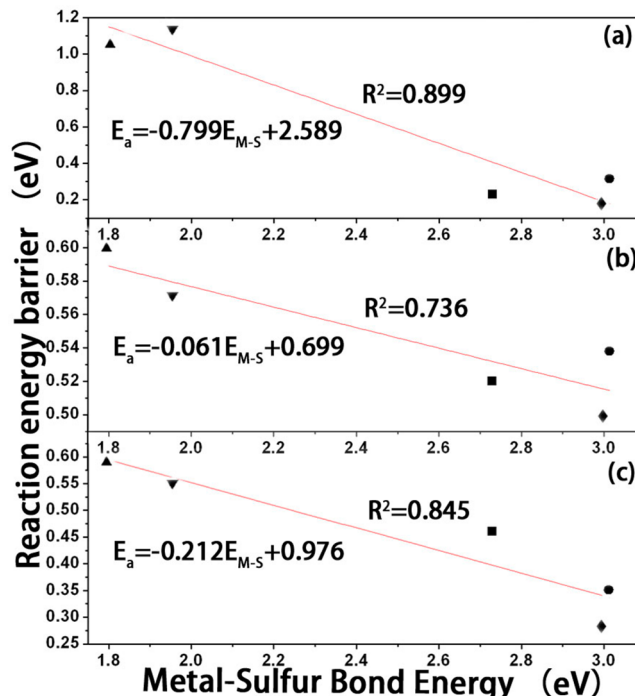


**Figure 9.** Relationship between metal–sulfur bond energy and the corresponding energy barrier of the hydrogen dissociation on the  $\text{Re}_2$  (a),  $\text{Re}_3$  (b), and  $\text{Re}_4$  (c) sites on various catalyst surfaces. The metal–sulfur bond energies of Re–S, Co–S, Ni–S, W–S, and Ta–S are adopted from ref 36. The symbols of  $\blacktriangle/\blacktriangledown/\blacklozenge/\bullet/\blacksquare$  denote the Re atom on Ni-/Co-/W-/Ta-promoted and promoter-free surfaces, respectively.

revelation to deepening the understanding and the recognition on the hydrogenation-catalyzed process.

#### 4. CONCLUSIONS

By means of DFT computations, hydrogen dissociation on the promoter-free and Co-, Ni-, W-, and Ta-promoted  $\text{ReS}_2$  catalysts have been studied theoretically. The surface structure and composition under the typical HDS conditions were first investigated by using a surface-phase diagram technique. It was shown that 25% S adsorption is the most stable for all the surfaces studied. Subsequently, hydrogen dissociations on these sulfided surfaces have been explored. It was found that hydrogen can be favorably dissociated at the Re site, and different promoters exhibited different effects on the activity of the nearest Re atom; i.e., Co, Ni passivates the nearest Re atom while W, Ta activates it. This activity difference has been ascribed to the different metal–S bonding strength. On going from promoter-free to promoted surface, the dissociation barrier of hydrogen at the  $S_a$  site decreases in the order promoter-free > W, Ta > Co, Ni, which can be rationalized by the p-bond center. The relatively high barrier demonstrates that the sulfided surfaces are robust. Furthermore, dissociation barriers at the interlayer are substantially high, independent of the dopant type, indicating that this pathway is nearly prohibited. In conclusion, we believe that this work moves toward a more rational understanding of the catalytic active transition-metal sulfide phase. It provides a basis for the research of HDS and HDN catalysts.

## ■ ASSOCIATED CONTENT

### ● Supporting Information

Figures S1–S5. The Supporting Information is available free of charge on the ACS Publications website at DOI: 10.1021/acs.jpcc.5b02710.

## ■ AUTHOR INFORMATION

### Corresponding Author

\*E-mail: huangyc@mail.ahnu.edu.cn. Tel: +(86-553-3937138).

### Notes

The authors declare no competing financial interest.

## ■ ACKNOWLEDGMENTS

This work was supported by the National Younger Natural Science Foundation of China No. 21203001 and Natural Science Foundation of China No. 21373012 (to S.F.W.) and Natural Science Foundation of Anhui Province No. 1408085MKL22. The numerical calculations in this paper have been performed on the supercomputing system in the Supercomputing Center of University of Science and Technology of China.

## ■ REFERENCES

- (1) Farag, H.; Whitehurst, D.; Sakanishi, K.; Mochida, I. Carbon Versus Alumina as a Support for Co–Mo Catalysts Reactivity Towards HDS of Dibenzothiophenes and Ddiesel Fuel. *Catal. Today* **1999**, *50*, 9–17.
- (2) Furimsky, E. Role of MoS<sub>2</sub> and WS<sub>2</sub> in Hydrodesulfurization. *Catal. Rev.: Sci. Eng.* **1980**, *22*, 371–400.
- (3) de Jong, K. P.; van den Oetelaar, L. C.; Vogt, E. T.; Eijssbouts, S.; Koster, A. J.; Friedrich, H.; de Jongh, P. E. High-Resolution Electron Tomography Study of an Industrial Ni-Mo/γ-Al<sub>2</sub>O<sub>3</sub> Hydrotreating Catalyst. *J. Phys. Chem. B* **2006**, *110*, 10209–10212.
- (4) Lauritsen, J.; Helveg, S.; Lægsgaard, E.; Stensgaard, I.; Clausen, B.; Topsøe, H.; Besenbacher, F. Atomic-Scale Structure of Co–Mo–S Nanoclusters in Hydrotreating Catalysts. *J. Catal.* **2001**, *197*, 1–5.
- (5) Byskov, L. S.; Nørskov, J. K.; Clausen, B. S.; Topsøe, H. DFT Calculations of Unpromoted and Promoted MoS<sub>2</sub>-Based Hydrodesulfurization Catalysts. *J. Catal.* **1999**, *187*, 109–122.
- (6) Schweiger, H.; Raybaud, P.; Kresse, G.; Toulhoat, H. Shape and Edge Sites Modifications of MoS<sub>2</sub> Catalytic Nanoparticles Induced by Working Conditions: A Theoretical Study. *J. Catal.* **2002**, *207*, 76–87.
- (7) Sun, M.; Nelson, A. E.; Adjaye, J. A DFT Study of WS<sub>2</sub>, NiWS, and CoWS Hydrotreating Catalysts: Energetics and Surface Structures. *J. Catal.* **2004**, *226*, 41–53.
- (8) Sun, M.; Nelson, A. E.; Adjaye, J. On the Incorporation of Nickel and Cobalt into MoS<sub>2</sub>-Edge Structures. *J. Catal.* **2004**, *226*, 32–40.
- (9) Chianelli, R.; Berhault, G.; Raybaud, P.; Kasztelan, S.; Hafner, J.; Toulhoat, H. Periodic Trends in Hydrodesulfurization: In Support of the Sabatier Principle. *Appl. Catal., A* **2002**, *227*, 83–96.
- (10) Räty, J.; Pakkanen, T. A Controlled Gas-Phase Preparation and HDS Activity of Re<sub>2</sub>(CO)<sub>10</sub> Alumina Catalysts. *Catal. Lett.* **2000**, *65*, 175–180.
- (11) Stern, E. W. Reaction Networks in Catalytic Hydrodenitrogenation. *J. Catal.* **1979**, *57*, 390–396.
- (12) Rodin, V.; Reddy, B.; Rao, V.; Kalinkin, A.; Startsev, A. Catalysis of Thiophene Hydrogenolysis by Bimetallic Sulfide Catalysts of Different Compositions. *React. Kinet. Catal. Lett.* **1989**, *40*, 71–76.
- (13) Escalona, N.; Ojeda, J.; Baeza, P.; García, R.; Palacios, J.; Fierro, J.; Agudo, A. L.; Gil-Llambías, F. Synergism between unsupported Re and Co or Ni Sulfide Catalysts in the HDS and HDN of Gas Oil. *Appl. Catal., A* **2005**, *287*, 47–53.
- (14) Kresse, G.; Hafner, J. Ab Initio Molecular Dynamics for Liquid Metals. *Phys. Rev. B: Condens. Matter Mater. Phys.* **1993**, *47*, 558.
- (15) Kresse, G.; Furthmüller, J. Efficient Iterative Schemes for Ab Initio Total-Energy Calculations Using a Plane-Wave Basis Set. *Phys. Rev. B: Condens. Matter Mater. Phys.* **1996**, *54*, 11169.
- (16) Kresse, G.; Joubert, D. From Ultrasoft Pseudopotentials to the Projector Augmented-Wave Method. *Phys. Rev. B: Condens. Matter Mater. Phys.* **1999**, *59*, 1758.
- (17) Blöchl, P. E. Projector Augmented-Wave Method. *Phys. Rev. B: Condens. Matter Mater. Phys.* **1994**, *50*, 17953.
- (18) Perdew, J. P.; Wang, Y. Accurate and Simple Analytic Representation of the Electron-Gas Correlation Energy. *Phys. Rev. B: Condens. Matter Mater. Phys.* **1992**, *45*, 13244.
- (19) Greeley, J.; Mavrikakis, M. Surface and Subsurface Hydrogen: Adsorption Properties on Transition Metals and Near-Surface Alloys. *J. Phys. Chem. B* **2005**, *109*, 3460–3471.
- (20) Perdew, J. P.; Burke, K.; Ernzerhof, M. Generalized Gradient Approximation Made Simple. *Phys. Rev. Lett.* **1996**, *77*, 3865.
- (21) Monkhorst, H. J.; Pack, J. D. Special Points for Brillouin-Zone Integrations. *Phys. Rev. B* **1976**, *13*, 5188.
- (22) Murray, H.; Kelty, S.; Chianelli, R.; Day, C. Structure of Rhodium Disulfide. *Inorg. Chem.* **1994**, *33*, 4418–4420.
- (23) Henkelman, G.; Überuaga, B. P.; Jónsson, H. A Climbing Image Nudged Elastic Band Method for Finding Saddle Points and Minimum Energy Paths. *J. Chem. Phys.* **2000**, *113*, 9901–9904.
- (24) Henkelman, G.; Jonsson, H. Improved Tangent Estimate in the Nudged Elastic Band Method for Finding Minimum Energy Paths and Saddle Points. *J. Chem. Phys.* **2000**, *113*, 9978–9985.
- (25) Raybaud, P.; Hafner, J.; Kresse, G.; Kasztelan, S.; Toulhoat, H. Ab Initio Study of the H<sub>2</sub>–H<sub>2</sub>S/MoS<sub>2</sub> Gas–Solid Interface: The Nature of the Catalytically Active Sites. *J. Catal.* **2000**, *189*, 129–146.
- (26) Wang, X.-G.; Chaka, A.; Scheffler, M. Effect of the Environment on α-Al<sub>2</sub>O<sub>3</sub> (0001) Surface Structures. *Phys. Rev. Lett.* **2000**, *84*, 3650.
- (27) Bollinger, M.; Jacobsen, K. W.; Nørskov, J. K. Atomic and Electronic Structure of MoS<sub>2</sub> Nanoparticles. *Phys. Rev. B: Condens. Matter Mater. Phys.* **2003**, *67*, 085410.
- (28) Schweiger, H.; Raybaud, P.; Toulhoat, H. Promoter Sensitive Shapes of Co (Ni) MoS Nanocatalysts in Sulfo-Reductive Conditions. *J. Catal.* **2002**, *212*, 33–38.
- (29) Raybaud, P.; Kresse, G.; Hafner, J.; Toulhoat, H. Ab Initio Density Functional Studies of Transition-Metal Sulphides: I. Crystal Structure and Cohesive Properties. *J. Phys.: Condens. Matter* **1997**, *9*, 11085.
- (30) Krebs, E.; Silvi, B.; Raybaud, P. Mixed Sites and Promoter Segregation: A DFT Study of the Manifestation of Le Chatelier's Principle for the Co (Ni) MoS Active Phase in Reaction Conditions. *Catal. Today* **2008**, *130*, 160–169.
- (31) Girleanu, M.; Alphazan, T.; Boudene, Z.; Bonduelle-Skrzypczak, A.; Legens, C.; Gay, A. S.; Copéret, C.; Ersen, O.; Raybaud, P. Magnifying the Morphology Change Induced by a Nickel Promoter in Tungsten (IV) Sulfide Industrial Hydrocracking Catalyst: A HAADF-STEM and DFT Study. *ChemCatChem* **2014**, *6*, 1594–1598.
- (32) Lee, K.; Murray, É. D.; Kong, L.; Lundqvist, B. I.; Langreth, D. C. Higher-accuracy Van Der Waals Density Functional. *Phys. Rev. B: Condens. Matter Mater. Phys.* **2010**, *82*, 081101.
- (33) Grimme, S. Semiempirical GGA-Type Density Functional Constructed with a long-Range Dispersion Correction. *J. Comput. Chem.* **2006**, *27*, 1787–1799.
- (34) Prodhomme, P.-Y.; Raybaud, P.; Toulhoat, H. Free-Energy Profiles along Reduction Pathways of MoS<sub>2</sub> M-edge and S-edge by Dihydrogen: A First-Principles Study. *J. Catal.* **2011**, *280*, 178–195.
- (35) Quartararo, J.; Mignard, S.; Kasztelan, S. Hydrodesulfurization and Hydrogenation Activities of Alumina-Supported Transition Metal Sulfides. *J. Catal.* **2000**, *192*, 307–315.
- (36) Toulhoat, H.; Raybaud, P.; Kasztelan, S.; Kresse, G.; Hafner, J. Transition Metals to Sulfur Binding Energies Relationship to Catalytic Activities in HDS: Back to Sabatier with First Principle Calculations. *Catal. Today* **1999**, *50*, 629–636.
- (37) Travert, A.; Nakamura, H.; van Santen, R. A.; Cristol, S.; Paul, J.-F.; Payen, E. Hydrogen Activation on Mo-based Sulfide Catalysts, a Periodic DFT Study. *J. Am. Chem. Soc.* **2002**, *124*, 7084–7095.

- (38) Kresse, G. Dissociation and Sticking of H<sub>2</sub> on the Ni (111), (100), and (110) Substrate. *Phys. Rev. B: Condens. Matter Mater. Phys.* **2000**, *62*, 8295.
- (39) van Helden, P.; van den Berg, J.-A.; Weststrate, C. J. Hydrogen Adsorption on Co Surfaces: A Density Functional Theory and Temperature Programmed Desorption Study. *ACS Catal.* **2012**, *2*, 1097–1107.
- (40) Kitchin, J.; Nørskov, J. K.; Barteau, M.; Chen, J. Modification of the Surface Electronic and Chemical Properties of Pt (111) by Subsurface 3d Transition Metals. *J. Chem. Phys.* **2004**, *120*, 10240–10246.
- (41) Pallassana, V.; Neurock, M.; Hansen, L. B.; Hammer, B.; Nørskov, J. K. Theoretical Analysis of Hydrogen Chemisorption on Pd (111), Re (0001) and Pd ML/R e (0001), Re ML/Pd (111) Pseudomorphic Overlayers. *Phys. Rev. B: Condens. Matter Mater. Phys.* **1999**, *60*, 6146.
- (42) Lee, Y.-L.; Kleis, J.; Rossmeisl, J.; Shao-Horn, Y.; Morgan, D. Prediction of Solid Oxide Fuel Cell Cathode Activity with First-Principles Descriptors. *Energy Environ. Sci.* **2011**, *4*, 3966–3970.
- (43) Hong, W. T.; Gadre, M.; Lee, Y.-L.; Biegalski, M. D.; Christen, H. M.; Morgan, D.; Shao-Horn, Y. Tuning the Spin State in LaCoO<sub>3</sub> Thin Films for Enhanced High-Temperature Oxygen Electrocatalysis. *J. Phys. Chem. Lett.* **2013**, *4*, 2493–2499.
- (44) Knudsen, K. G.; Cooper, B. H.; Topsøe, H. Catalyst and Process Technologies for Ultra Low Sulfur Diesel. *Appl. Catal., A* **1999**, *189*, 205–215.
- (45) Nørskov, J.; Clausen, B.; Topsøe, H. Understanding the Trends in the Hydrodesulfurization Activity of the Transition Metal Sulfides. *Catal. Lett.* **1992**, *13*, 1–8.